THE JOURNAL OF PHYSICAL CHEMISTRY B

Article

pubs.acs.org/JPCB

Strong Isotope Effects on Effective Interactions and Phase Behavior in Protein Solutions in the Presence of Multivalent Ions

Michal K. Braun,[†] Marcell Wolf,[†,⊥] Olga Matsarskaia,[†] Stefano Da Vela,[†] Felix Roosen-Runge,[‡,#] Michael Sztucki,[§] Roland Roth,[∥] Fajun Zhang,[*,†] and Frank Schreiber[†]

[†]Institut für Angewandte Physik, Universität Tübingen, Auf der Morgenstelle 10, 72076 Tübingen, Germany

[‡]Institut Laue-Langevin, 71 Avenue des Martyrs, 38000 Grenoble, France

[§]ESRF - The European Synchrotron, 71 Avenue des Martyrs, 38000 Grenoble, France

[∥]Institut für Theoretische Physik, Universität Tübingen, Auf der Morgenstelle 14, 72076 Tübingen, Germany

Supporting Information

ABSTRACT: In this article, we have studied the influence of the isotopic composition of the solvent (H_2O or D_2O) on the effective interactions and the phase behavior of the globular protein bovine serum albumin in solution with two trivalent salts ($LaCl_3$ and YCl_3). Protein solutions with both salts exhibit a reentrant condensation phase behavior. The condensed regime (regime II) in between two salt concentration boundaries ($c^* < c_s < c^{**}$) is significantly broadened by replacing H_2O with D_2O. Within regime II, liquid−liquid phase separation (LLPS) occurs. The samples that undergo LLPS have a lower critical solution temperature (LCST). The value of LCST decreases significantly with increasing solvent fraction of D_2O. The effective protein−protein interactions characterized by small-angle X-ray scattering demonstrate that although changing the solvent has negligible effects below c^*, where the interactions are dominated by electrostatic repulsion, an enhanced effective attraction is observed in D_2O above c^*, consistent with the phase behavior observed. As the LCST−LLPS is an entropy-driven phase transition, the results of this study emphasize the role of entropy in solvent isotope effects.

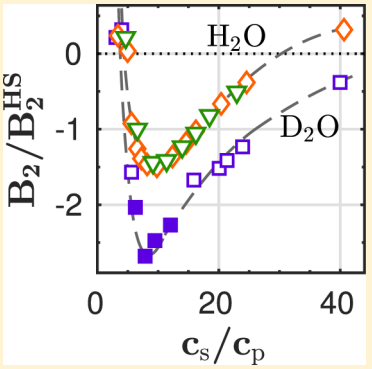

INTRODUCTION

Quantitative description of the effective protein−protein interactions in aqueous solutions is one of the major challenges in the study of soft and biological matter.[1−6] As the effective interactions control the exact phase behavior of protein solutions, including crystallization, a complete picture of protein interactions at different length scales with various control parameters could ease the search of optimal conditions for crystal growth. Protein phase behavior is also crucial for a better understanding of protein aggregation-related physiological diseases. In particular, the existence of a metastable liquid−liquid phase separation (LLPS) in protein solutions is a fundamental biophysical phenomenon and provides a mechanism for biological structure formation.[1,3,6−11] It serves as a prerequisite for the formation of crystals in cataracts[7,10,11] and for fibers responsible for sickle cell anemia and Alzheimer's disease[1,8] and influences the pathways of protein crystallization.[3,12,13]

Effective interactions of biological macromolecules in aqueous solution are generally complex. They depend on a number of environmental parameters,[4−6,14−24] such as the concentration and valence of salt ions, the type of salt (e.g., Hofmeister series), the concentration of additives (e.g., nonadsorbing polymers and co-solvents), pH, and temperature. Possible mechanisms to change protein interactions are, among others, the control of protein surface charge and the tuning of hydrophobic and hydrophilic interactions. Furthermore, there is a whole arsenal of different types of interactions, including Coulombic interaction, hydrogen-bond formation, hydrophobic interaction, and the formation of salt bridges, which may be either highly specific or nonspecific. The diversity of interactions leads to a rich phase behavior in protein solutions. Despite the complexity, progress has been made in modeling the liquid−liquid phase transition in protein and colloid systems, emphasizing the role of short-ranged attractions.[12,13,18,25−28]

Among the various environmental parameters, the solvent isotope effect on the effective interactions between proteins is still far from clear. The impact of the isotopic composition of the solvent strongly depends on the circumstances and the observable of interest. The physicochemical properties of D_2O are very similar to those of H_2O. It is thus commonly believed that the substitution of H_2O with D_2O causes only a very small perturbation of the structural preferences of a solute. In fact, in many biophysical studies using neutron scattering and infrared and NMR spectroscopy, D_2O is widely used as the solvent to obtain a useful signal.[29,30] In all these studies, it is generally

Received: December 21, 2016
Published: February 13, 2017

DOI: 10.1021/acs.jpcb.6b12814
J. Phys. Chem. B 2017, 121, 1731−1739

assumed that D_2O has a negligible effect on the structure and interactions of these biological systems. However, while the effect of D_2O is generally considered weak in biological systems, studies have shown significant changes in the interactions between proteins and their dynamics when H_2O is substituted with D_2O. For instance, it has been found that D_2O can stabilize proteins against thermal denaturation[31−36] and influence the macromolecular dynamics in *Escherichia coli*.[37]

Some studies have found that the effective protein−protein attraction can be enhanced when H_2O is replaced by D_2O.[29,30,38,39] Gripon et al. investigated the effective interactions in lysozyme solutions in H_2O and D_2O to understand the lower solubility of lysozyme in D_2O. The solubility line is shifted to higher temperatures by about 7.2 °C in D_2O. SANS measurements and data analysis based on the second virial coefficient indicate that the repulsive potential due to the net surface charge does not change. The attraction between lysozyme molecules, however, is stronger in D_2O than in H_2O. It is assumed that this is due to hydrophobic hydration and salt-specific interactions.

A recent study by Bucciarelli et al.[30] on γ_B-crystallin solutions has shown an even stronger solvent isotope effect. Replacing H_2O with D_2O results in an increase of the critical LLPS temperature of up to 16 °C. While this systematic study demonstrates that the variation of the critical temperature can be described using the extended law of corresponding states,[27,40] the underlying physical mechanism of the solvent isotope effect is still not clear.[30]

We have shown previously that trivalent salts, such as YCl_3, can induce a reentrant condensation (RC) phase behavior in several acidic proteins.[41−45] For a given protein concentration c_p, when the salt concentration c_s is below a certain value c^*, or above a value c^{**} (with $c^* < c^{**}$), protein solutions are clear. At salt concentrations between c^* and c^{**}, protein condensation occurs, including aggregation or clustering, LLPS, and crystallization.[46−49] In particular, the metastable LLPS has been demonstrated to be an entropy-driven process, as the system exhibits a lower critical solution temperature (LCST) phase behavior.[50] The charge inversion and the effective attraction mediated via multivalent metal ions have been further investigated by experiments, simulations, and theoretical studies.[43,45,51−55] However, in spite of the details known about the macroscopic phase behavior and the interactions, the microscopic origin of the short-ranged attraction is not yet completely clear.[46,50]

In this work, we perform a systematic study of the effective interactions and the phase behavior of the protein bovine serum albumin (BSA) in solution with two different trivalent salts (YCl_3 and $LaCl_3$) in both H_2O and D_2O. Our goal is to explore the solvent isotope effect on the effective interactions and on the phase behavior, which may shed light on the underlying mechanism of the solvent isotope effect and the entropy-driven LLPS.

EXPERIMENTAL SECTION

Material and Sample Preparation. BSA (product no. A7906), $LaCl_3$ (product no. 298182), YCl_3 (product no. 451363), and D_2O were purchased from Sigma-Aldrich and used as received. For the stock solutions, protein and salt were dissolved in D_2O or degassed Milli-Q H_2O (conductivity 18.2 MΩ cm).

The state diagrams of protein solutions with $LaCl_3$ at room temperature in D_2O and H_2O were determined by visual inspection or ultraviolet−visible (UV−vis) transmission measurements. In H_2O, samples in regime II became difficult to judge by eye, as samples turned only slightly turbid in regime II and no macroscopic phase separation occurred. Therefore, UV−vis transmission measurements (Cary UV−vis spectrophotometer 50 Scan, Varian Australia Pty Ltd) were used to determine the boundaries of regime II. This method worked very well for BSA concentrations up to 100 mg/mL. Example plots of the UV−vis transmission measurements and the determination of boundaries are presented in Figure S1. For higher protein concentrations (e.g., 150 mg/mL), the boundaries were determined by visual inspection again. The state diagram of protein solutions with YCl_3 and different solvent fractions of D_2O was determined by visual inspection. To discriminate between LLPS and aggregation, the turbid samples were examined using a transmission microscope (AxioScope A1, Zeiss) equipped with an AxioCam ICc5 charge-coupled device (CCD) camera.

Determination of the LCST. The dependence of the transition temperature on the solvent fraction of D_2O was determined using a UV−vis spectrometer equipped with a water bath for temperature control (Haake A10B and SC 150, Thermo Fisher Scientific Inc.). The sample was slowly heated from the bath temperature of 12 °C at a rate of 0.1 C/min. The temperature of the sample solution was calibrated using a thermocouple attached to the sample holder. At a heating rate of 0.1 °C/min, the sample temperature was given by $T_s = (0.092t + 12)$ °C, with time t (in minutes) after the start of the experiment. The absorbance spectra in the range of 500−800 nm were collected every 2 min, and the intensities were integrated and plotted against temperature. The LCST was determined from the main peak of the first derivative of the integrated absorbance as a function of temperature. Before the UV−vis measurement, the samples were centrifuged for 2 min with an RCF of 6860g to remove large aggregates.

Small-Angle X-ray Scattering (SAXS). Effective protein−protein interactions in the solutions were characterized by SAXS. SAXS experiments were conducted at beamline ID02 at the ESRF, Grenoble, France. The X-ray energy was 12 keV, which corresponds to a wavelength of 1.0 Å. For all measurements, the sample-to-detector distance was set to 2 m, covering a q-range of 0.005−0.5 $Å^{-1}$. The data were collected by a high-sensitivity fiber-optic-coupled CCD detector placed in an evacuated flight tube. The samples were prepared right before the measurement. The protein solution was loaded into a flow-through quartz capillary with a diameter of 2 mm and a wall thickness of 0.01 mm. The data sets were reduced by subtracting the scattering of a pure salt solution as a background and by normalizing to absolute intensity. Further details on q-resolution, calibration, and data reduction can be found in refs 56 and 57. Data fitting was performed using IGOR Pro with macros provided by NIST.[58]

RESULTS

Phase Behavior and Effective Interactions of BSA−$LaCl_3$ in H_2O and D_2O. We first present the phase behavior of BSA with $LaCl_3$ in both pure H_2O and D_2O at room temperature. As shown in Figure 1, an RC is found in both cases.[41] The solutions are clear below the salt concentration c^* (regime I). In between c^* and c^{**} (with $c^{**} \gg c^*$), condensation takes place, which is the so-called regime II.

DOI: 10.1021/acs.jpcb.6b12814
J. Phys. Chem. B 2017, 121, 1731−1739

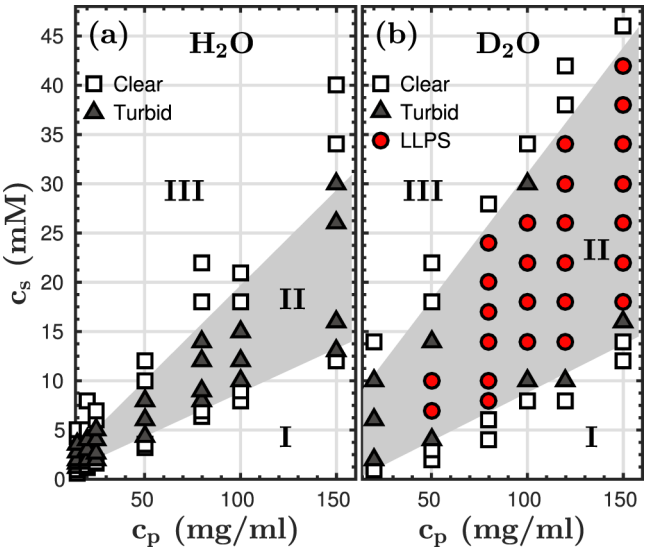

Figure 1. Experimental state diagram of the BSA–$LaCl_3$ system at room temperature in H_2O (a) and D_2O (b). Shaded areas correspond to the condensed regime.

Above the salt concentration, c^{**}, the protein solutions reclarify (regime III). However, the macroscopic appearance of the solutions in regime II is different in H_2O and D_2O. Solutions in H_2O are only slightly turbid between c^* and c^{**}. There is no macroscopic phase separation and no LLPS. After a few hours, small precipitates become visible at the bottom or on the wall of the cuvette. In D_2O, the solutions are highly turbid and phase-separate macroscopically. Amorphous protein aggregates or droplets with a high protein density form right after mixing and sediment quickly. Figure 1 also shows that when replacing H_2O with D_2O the area of regime II is significantly enlarged. A closer look at the two boundaries reveals that the c^* values are very similar in both cases. The value of c^{**}, however, is higher in D_2O than in H_2O.

Figure 2 presents the plots of the integrated UV–vis absorbance of the samples with 80 mg/mL BSA, 13 mM $LaCl_3$, and solvent fractions of D_2O from 0 to 0.3 as a function of temperature. At the starting temperature, 12.0 °C, and after centrifugation, all sample solutions are clear with an integrated absorbance close to zero. When increasing the temperature, a significant increase of the apparent absorbance occurs. The transition from low to high absorbance becomes sharper with increasing D_2O solvent fraction. The first derivative of the absorbance curve as a function of temperature was used to determine the exact LCST value, as shown in Figure 2b. The peak position, that is, the LCST of each sample, is plotted as a function of D_2O solvent fraction in Figure 2c. When the D_2O solvent fraction increases, this transition temperature (the LCST) decreases dramatically. At a D_2O solvent fraction of 0.10, this value decreased from 31.5 to 26.8 °C. Up to a D_2O solvent fraction of 0.20, the transition temperature decreases linearly. The slight deviation from the linear behavior at a higher D_2O solvent fraction may be due to the formation of small amounts of protein aggregates, as the protein concentration after centrifugation decreases with increasing D_2O solvent fraction (Table 1). At the highest investigated D_2O solvent fraction of 0.3, the LCST decreased to 18.7 °C, which is already 12.8 °C lower than that in pure H_2O. A further decrease of the LCST with increasing D_2O solvent fraction is expected. Because of the protein aggregation, it is difficult to

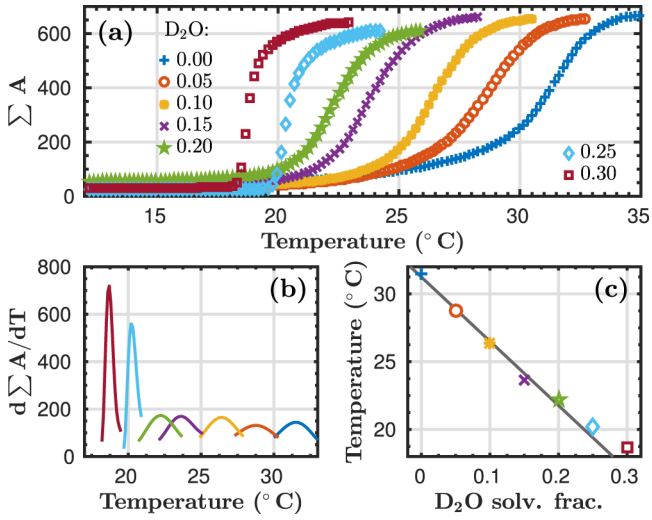

Figure 2. LCST phase behavior of 80 mg/mL BSA with 13 mM $LaCl_3$. (a) Integrated absorbance ($\sum A$) (500–800 nm) vs temperature for different D_2O solvent fractions. (b) First derivative of the integrated absorbance with respect to temperature. The maximum determines the transition temperature. (c) Transition temperature as a function of D_2O solvent fraction. The line is a linear fit to the first five data points.

Table 1. Determination of the LCST for a Series of Samples with 80 mg/mL BSA, 13 mM $LaCl_3$, and Different D_2O Solvent Fractions

D_2O solv. frac.	0	0.05	0.10	0.15	0.20	0.25	0.30
c_p (mg/mL)	80.1	80.7	80.8	80.1	80.4	72.1[a]	77.1[a]
LCST (°C)	31.5	28.8	26.4	23.6	22.2	19.7	18.7

[a]Underlined numbers indicate a decrease of protein concentration in the supernatant due to aggregation.

investigate higher D_2O solvent fractions with our method. From a linear fit of the first five data points shown in Figure 2c, an LCST of −16.1 °C is estimated in pure D_2O. This would be 47.6 °C below the LCST in pure H_2O.

Effective Protein–Protein Interactions Characterized by SAXS. For a quantitative understanding of the solvent isotope effects, we characterize the effective protein–protein interactions using SAXS. Representative SAXS profiles are shown in Figure 3 for BSA–$LaCl_3$ solutions in both H_2O and D_2O as a function of salt concentration. In both cases, SAXS data show similar trends. At low salt concentration, the effective protein–protein interactions are dominated by the net negative charge. A strong correlation peak is visible. With increasing salt concentration, the low q intensity increases, indicating the reduction of repulsion. In this region of the phase diagram (regime I), the solutions are clear.

With further increasing salt concentration, the systems become more and more dominated by attractive interactions, with the attraction reaching its maximum at 12 mM (H_2O) and 20 mM $LaCl_3$ (D_2O). In H_2O, starting from 15 mM, the strength of the attraction starts to decrease. In D_2O, the strength of the attraction starts to decrease at 25 mM. In D_2O, the decrease starts at a higher salt concentration, which corresponds very well to the finding that regime II also extends to higher salt concentrations (see also Figure 1). The decrease is found to start very close to the upper boundaries (c^{**}) of the second regime. In H_2O, c^{**} (80 mg/mL) is located at 16 ± 2 mM. In D_2O, c^{**} (87 mg/mL) is located at 26 ± 2 mM. The

DOI: 10.1021/acs.jpcb.6b12814
J. Phys. Chem. B 2017, 121, 1731–1739

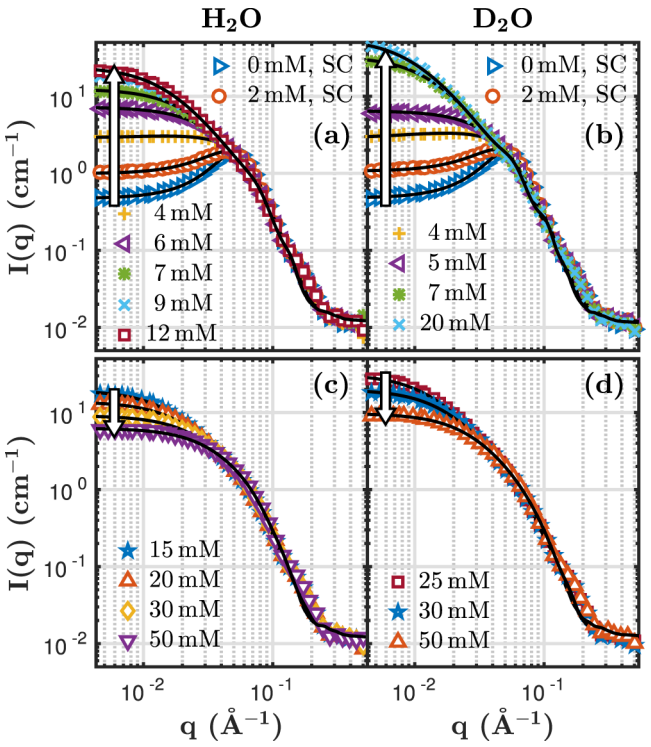

Figure 3. (a, c) SAXS data with model fits for samples in H_2O containing 85 mg/mL BSA. (b, d) SAXS data with model fits for samples in D_2O containing 87 mg/mL BSA. The scattering intensity at low q increases with increasing salt concentration in (a) and (b) and decreases in (c) and (d). In the legend, SC indicates that the screened Coulombic potential was used for data fitting. The other data were fitted using the SHS potential. For further information on the SAXS data analysis, see the Supporting Information.

data with decreasing low q intensity are shown in the lower parts of the figure. SAXS profiles for a further set of data with 150 mg/mL BSA are shown in Figure S2.

To quantify the effective interactions, the SAXS data were fitted using models with an ellipsoid form factor and different interaction potentials. Figure 3 presents the SAXS data with model fitting for BSA−$LaCl_3$ in H_2O and D_2O, respectively. The fits are superimposed on the data as solid black lines. The corresponding structure factors are shown in Figure S3. In both cases, below c^*, the interactions are dominated by electrostatics due to the surface charges. The two scattering curves for samples with very low salt concentrations (0 and 2 mM $LaCl_3$) were fitted using a screened Coulombic potential in both H_2O and D_2O. In H_2O, the fitted charges are 18.1 and 10.3e and the ionic strengths are 7.4 and 10 mM for 0 and 2 mM, respectively. In D_2O, the charges are 16.3 and 8.71e and the ionic strengths are 6.2 and 8.6 mM for 0 and 2 mM, respectively. The values in H_2O are thus very similar to those in D_2O. Therefore, the *repulsive* part of the potential shows only a weak dependence on the solvent (H_2O or D_2O).

In regimes II and III, where the effective interactions are *attractive*, a strong isotope effect is observed. This interesting finding will be further discussed and explained in the Discussion section.

To quantitatively describe the attractive potential, the sticky hard sphere (SHS) potential was used.[59] A pertubative solution of the Percus−Yevick closure relation was used to calculate the structure factor.[60] The SHS model was introduced by Baxter[59] for a system with hard-core repulsion and additional short-range attraction, which can undergo fluid−vapor phase separation. The interaction potential for particles with radius R is

$$\beta U(r) = \begin{cases} \infty & r < \sigma = 2R \\ -\beta u_0 = \ln\left(\dfrac{12\tau\Delta}{\sigma+\Delta}\right) & \sigma < r < \sigma + \Delta \\ 0 & r > \sigma + \Delta \end{cases} \quad (1)$$

with units of k_BT ($\beta = 1/k_BT$), where τ is the stickiness parameter and Δ is the width of the square well.

Frequently, for simplicity, the limit $\Delta \to 0$ is considered. In this limit, the reduced second virial coefficient is given by

$$\lim_{\Delta\to 0} \frac{B_2}{B_2^{HS}} = 1 - \frac{1}{4\tau} \quad (2)$$

$B_2^{HS} = 16\pi R^3/3$ is the second virial coefficient of a hard sphere of radius R. For the SAXS data fitting, Δ was fixed to 0.01σ to avoid artificial coupling with τ. Theoretical considerations and computer simulations[27,61,62] suggest that there is a universal value of $B_2/B_2^{HS} \approx -1.5$ at the critical point of the gas−liquid transition for various systems.

Figure 4 summarizes the B_2/B_2^{HS} values calculated from the stickiness parameter obtained for samples in regimes II and III.

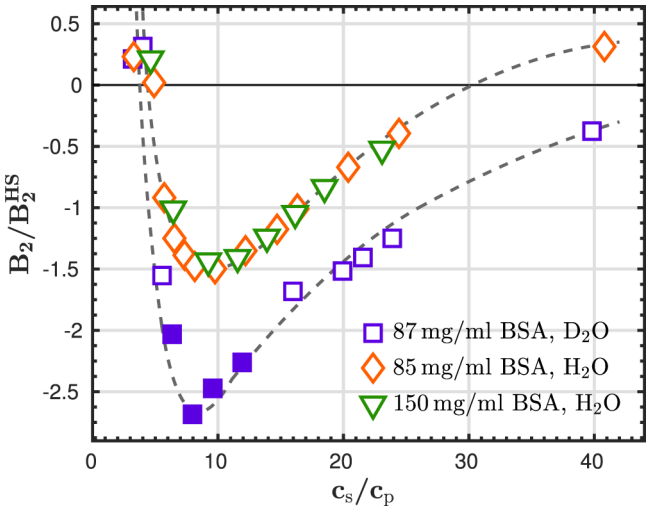

Figure 4. Reduced 2nd virial coefficients calculated from the SAXS data analysis of BSA−$LaCl_3$ samples (Figure 3) B_2/B_2^{HS} was calculated for samples above c^*. Triangles and diamonds denote samples in H_2O. Samples in D_2O are denoted by squares. Solid squares indicate samples showing LLPS. The dashed lines are guides to the eye.

The data are plotted against the normalized salt concentration, c_s/c_p. Results for two sets of samples with 150 and 85 mg/mL BSA in H_2O and one set of samples with 87 mg/mL BSA in D_2O are shown. Dashed lines are added as guides to the eye. Remarkably, the two series measured for the BSA−$LaCl_3$ system in H_2O fall onto one common master curve. In H_2O, B_2/B_2^{HS} only touches −1.5 in its minimum. Clearly, the curve in D_2O is well below the one in H_2O. Thus, the strength of attraction is significantly enhanced in D_2O. The samples that showed macroscopic LLPS are marked by filled squares. B_2/B_2^{HS} for these samples is below −1.5, which is in agreement with the findings reported by Wolf et al.[62] Furthermore, B_2/B_2^{HS} first decreases quickly above c^*. After reaching the minimum, it starts to increase again but much more slowly. This

DOI: 10.1021/acs.jpcb.6b12814
J. Phys. Chem. B 2017, 121, 1731−1739

nonsymmetric change is most likely attributed to the screening effect of the co-ion, Cl^-. The increasing amount of co-ions screens the effective surface charge of the proteins. Fujihara and Akiyama studied the attractive interaction between macroanions mediated by divalent cations and observed a similar trend of effective interaction potential as a function of cation concentration.[52,54]

This quantitative interpretation and analysis of the SAXS data nicely fits to the qualitative macroscopic phase behavior in the different systems described above (Figure 1). The qualitative observations as well as the quantitative results show that the attraction is enhanced when H_2O is replaced by D_2O.

Effect of D_2O Solvent Fraction on the Phase Behavior and the Effective Interactions. The general phase behavior, including LCST for BSA with YCl_3 in H_2O, has been described in our previous work.[41,46,50] Here, we focus on the effect of the solvent fraction of D_2O on the phase behavior. We first determined a state diagram for protein solutions with a fixed protein concentration (91.7 mg/mL BSA) as a function of the YCl_3 concentration and the solvent fraction of D_2O. The results are summarized in Figure 5. The shaded area indicates regime

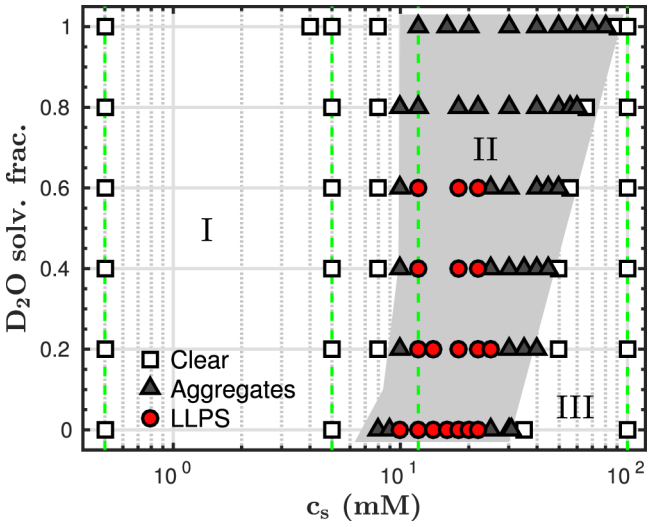

Figure 5. Experimental state diagram for BSA with YCl_3 at different solvent fractions of D_2O. The BSA concentration was fixed at 91.7 mg/mL. The shaded area corresponds to regime II. Sample series with selected salt concentrations for SAXS measurements were marked by green lines.

II. This state diagram shows that above a D_2O solvent fraction of 0.8 there is no LLPS anymore but only amorphous aggregation. For example, samples with 12 mM YCl_3 are all in the condensed regime (labeled with dashed green line). With increasing solvent fraction of D_2O, the condensed phase undergoes a transition from dense liquid droplets to amorphous protein aggregates. A direct observation of the morphology of the condensed phase using optical microscopy is presented in Figure S4. In addition to the structural change of the condensed phase, we observe a shift of the c^{**} boundary to higher salt concentrations with increasing solvent fraction of D_2O. The location of the c^* boundary stays more or less constant.

To further investigate the solvent isotope effect on the effective interactions, four series of samples with salt concentrations well below c^*, close to c^*, in regime II (between c^* and c^{**}), and slightly above c^{**} were measured by SAXS as a function of the D_2O solvent fraction. The salt concentrations that were chosen for the SAXS experiments are marked by green lines in Figure 5. The measured SAXS profiles are shown in Figure 6.

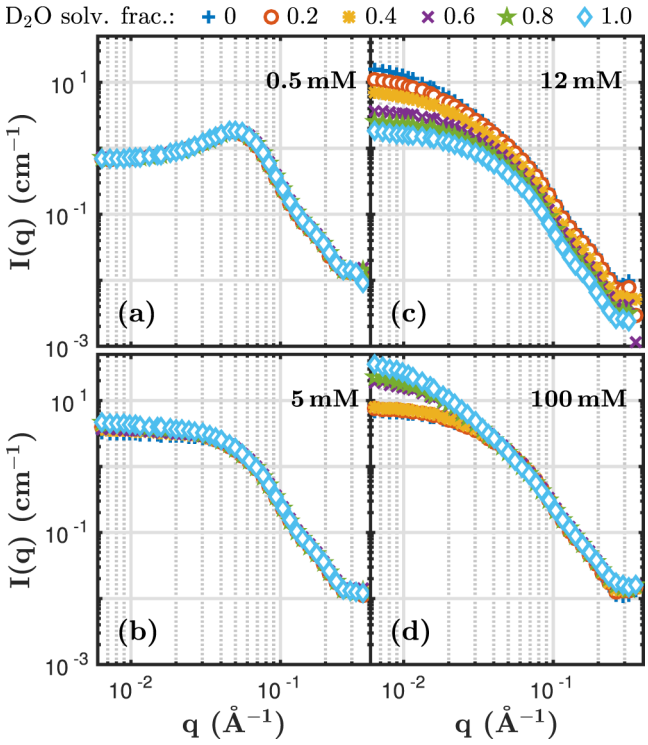

Figure 6. SAXS profiles for samples in different regimes with BSA 91.7 mg/mL and varying solvent fractions of D_2O. The YCl_3 concentrations are given in each subplot (see also green dashed lines in Figure 5).

Well below c^*, at c_s = 0.5 mM YCl_3, the scattering curves exhibit a correlation peak. This is the result of the long-range Coulombic repulsion due to the net negative charge of the proteins. Varying the D_2O solvent fraction does not affect the scattering profiles and thus the effective interactions. This is in good agreement with the results for BSA with $LaCl_3$ at low salt concentrations, which are presented in Figure 3.

Slightly below c^* with c_s = 5 mM YCl_3, the correlation peak in the SAXS profiles vanishes. An increase in the D_2O solvent fraction slightly shifts the scattering intensity at low q to higher values, indicating a slight increase in the attractive interactions.

In regime II with 12 mM YCl_3, where macroscopic phase separation occurs as shown in Figure 5, the samples were centrifuged, and only the supernatant was used for SAXS measurements. The vertical shift of the SAXS profiles corresponds to the variation of the protein concentration in the supernatant. The downward shift of the SAXS profiles with increasing D_2O solvent fraction is consistent with an increase of attraction.

In regime III with 100 mM YCl_3, where the samples are clear again, the scattering intensity at low q and hence the attraction increase significantly with increasing D_2O solvent fraction. This is also consistent with the macroscopic observation that the samples are closer to c^{**} with increasing D_2O solvent fraction (Figure 5).

DOI: 10.1021/acs.jpcb.6b12814
J. Phys. Chem. B 2017, 121, 1731−1739

DISCUSSION

We have studied the solvent isotope effect (H_2O vs D_2O) on the phase behavior of BSA solutions in the presence of two trivalent salts, $LaCl_3$ and YCl_3. While the RC phase behavior is found under all experimental conditions (salt or solvent), LCST−LLPS occurs only under certain conditions. The phase behaviors found in different systems are summarized in Table 2.

Table 2. Summary of LCST−LLPS Phase Behavior at Room Temperature

no.	solvent	salt	macroscopic phase behavior in regime II	attraction
1	H_2O	$LaCl_3$	mesoscopic clusters	too weak for LLPS
2	D_2O	$LaCl_3$	LCST−LLPS	suitable for LLPS
3	H_2O	YCl_3	LCST−LLPS	suitable for LLPS
4	D_2O	YCl_3	amorphous aggregates	too strong for LLPS

In the BSA−YCl_3 system, LLPS occurs in pure H_2O. At room temperature, the region of LLPS shrinks with increasing D_2O solvent fraction until it vanishes in pure D_2O. In the BSA−$LaCl_3$ system, however, LLPS occurs in pure D_2O at room temperature, whereas in pure H_2O, LLPS occurs only at temperatures above 30 °C (Figure 2). At room temperature, only mesoscopic protein clusters exist, and there is no macroscopic phase separation.

The effective protein−protein interactions characterized by SAXS demonstrate that the attraction increases by replacing H_2O with D_2O (Figure 4). This explains the phase behavior that is summarized in Table 2. In BSA−$LaCl_3$ in H_2O, there is no LLPS at room temperature because the attraction is too weak. In BSA−YCl_3 in D_2O, there is no LLPS because the attraction is too strong and only amorphous aggregates are formed.

The significant decrease of the LCST with increasing D_2O solvent fraction should be compared with the effects of the solvent isotope on the solubility of lysozyme. A difference of about 7.2 °C in D_2O versus H_2O was reported.[29,38] In another system, namely, in solutions of γ_B-crystallin, the (upper) critical temperature of LLPS increases by 16 °C in D_2O versus H_2O.[30] As the 7.2 °C difference in protein solubility of lysozyme is consistent with the temperature difference of the maximum density of light and heavy water, the larger difference observed in γ_B-crystallin solutions and in the work presented here indicates that other contributions may play a crucial role.

The existence of an LCST phase behavior in our systems demonstrates that the LLPS is driven by entropy. Thus, the observed significant response of the effective interactions (mainly the attractive part) to the solvent composition in protein solutions must be due to the solvent-isotope-dependent entropy contribution. Before discussing further the possible entropy contribution, we emphasize that the protein condensation observed is not caused by a change of the protein structure induced by YCl_3 or $LaCl_3$. We have studied the stability of the protein secondary structure in the presence of multivalent salts in H_2O and D_2O using circular dichroism (CD) and Fourier transform infrared.[42,57,63] The consistency of the results of the different techniques suggests that replacing H_2O with D_2O has no significant effect on the secondary structure of proteins. Moreover, the successful growth of high-quality crystals and structural analysis confirm that the proteins are still in their native state.[47,63,64]

We have recently discussed the mechanism of the LCST phase behavior in our system using the patchy colloid model. We propose that the key entropy contribution is due to the release of hydration water molecules upon ion bridging.[50] Upon heating, both the carboxy groups and the trivalent ions are partially dehydrated, resulting in a high entropy gain. Substitution of H_2O with D_2O certainly influences the hydration and dehydration of both proteins and cations. Unfortunately, studies on the hydrogen bonds in H_2O or D_2O for systems involving different types of functional groups turn out to be a great challenge.[31,65−68] Nevertheless, we find that these isotope effects lead to a higher entropy contribution for our system in D_2O, which results in an enhanced effective attraction between proteins and a lower LCST. The entropy contribution to the solvent isotope effects may also shed light on the unusual strong effects observed in other protein systems.[29,30,38]

It is worth noting that although similar entropy-driven LCST phase behavior is common in some polymer solutions, the isotope effects of the solvents are different. In some polymer solutions (e.g., PNIPAM), replacing H_2O with D_2O *increases* the LCST by 1 or 2 °C,[69,70] which is in contrast to our system, where we observe a *significant decrease* in the LCST. This opposite trend of the solvent isotope effect may be due to the different types of entropy contributions involved. In aqueous solutions of polymers, the entropy contribution comes from the dehydration of the hydrophobic part of the molecules.[70,71] Therefore, the stability of this hydration shell is enhanced when H_2O is replaced by D_2O, leading to a higher LCST. In our system, the entropy contribution comes from the reduced translational and rotational entropy of the hydration waters of the hydrophilic carboxyl groups on the protein surface and the metal cations. The different significance of the solvent isotope effect between the polymer and protein systems might be due to the different levels of cooperation of the hydrogen bond or the different amounts of hydration water involved.

CONCLUSIONS

In this work, we have studied the effective protein−protein interactions and phase behavior in solutions with two trivalent salts ($LaCl_3$ and YCl_3). In particular, we focused on the solvent isotope effect when replacing H_2O with D_2O. For both systems in both solvents, an RC phase behavior is observed. Within regime II, LCST−LLPS occurs under certain specific conditions. This rich phase behavior is highly sensitive to the D_2O solvent fraction. While c^* is weakly affected by replacing H_2O with D_2O, c^{**} shifts to higher salt concentrations, resulting in a broadening of regime II. The LCST−LLPS phase behavior for both salts shows strong solvent isotope effects, as summarized in Table 2. The LCST decreases significantly with increasing D_2O solvent fraction. The effective protein−protein interactions characterized by SAXS are consistent with the phase behavior observed. At low salt concentrations below c^*, interactions are dominated by electrostatic repulsion, which is not sensitive to the D_2O solvent fraction. Above c^*, the effective interactions become attractive and strongly depend on the D_2O solvent fraction. The interaction potential can be well described using a SHS model, indicating the short-ranged nature of the attraction. The reduced second virial coefficients, B_2/B_2^{HS}, decrease steeply first and increase slowly after reaching a minimum with increasing salt concentration. Similar trends are observed in both H_2O and D_2O, but the values become more negative in D_2O, indicating an enhanced attraction. The

DOI: 10.1021/acs.jpcb.6b12814
J. Phys. Chem. B 2017, 121, 1731−1739

entropy-driven LCST phase behavior suggests that the origin of the short-ranged attraction is closely related to entropy, which is most likely due to the release of hydration water from both metal ions and protein surfaces upon ion binding.[50] The entropy contribution to the solvent isotope effects may also shed light on the unusual strong effects observed in other protein systems.[29,30,38]

■ ASSOCIATED CONTENT

Supporting Information

The Supporting Information is available free of charge on the ACS Publications website at DOI: 10.1021/acs.jpcb.6b12814.

Details on SAXS data fitting, determination of the LCST using UV−vis transmission, data for 150 mg/mL BSA, structure factors obtained from data fitting, series of microscope images for samples with varying D_2O solvent fraction (PDF)

■ AUTHOR INFORMATION

Corresponding Author

*E-mail: fajun.zhang@uni-tuebingen.de.

ORCID

Michal K. Braun: 0000-0002-9642-7492

Fajun Zhang: 0000-0001-7639-8594

Present Addresses

[⊥]Austrian SAXS Beamline, ELETTRA Sincrotrone, Outstation of the Institut für Anorganische Chemie, Technische Universität Graz, Streymayrgasse 9/V, 8010 Graz, Trieste, Italy (M.W.).

[#]Division of Physical Chemistry, Department of Chemistry, Lund University, Naturvetarvägen 16, 22400 Lund, Sweden (F.R.-R.).

Notes

The authors declare no competing financial interest.

■ ACKNOWLEDGMENTS

The authors thank R. Akiyama (Kyushu University, Japan) and G. Lotze (ESRF) for valuable discussions and help for data analysis. This work was supported by the Deutsche Forschungsgemeinschaft (DFG). Furthermore, they thank the ESRF for allocation of beamtime on ID02. Olga Matsarskaia acknowledges a studentship by the Studienstiftung des Deutschen Volkes.

■ REFERENCES

(1) Gunton, J.; Shiryayev, A.; Pagan, D. *Protein Condensation: Kinetic Pathways to Crystallization and Disease*; Cambridge University Press, 2007.

(2) Durbin, S. D.; Feher, G. Protein crystallization. *Annu. Rev. Phys. Chem.* **1996**, *47*, 171−204.

(3) Vekilov, P. G. Dense Liquid Precursor for the Nucleation of Ordered Solid Phases from Solution. *Cryst. Growth Des.* **2004**, *4*, 671−685.

(4) Piazza, R. Interactions and phase transitions in protein solutions. *Curr. Opin. Colloid Interface Sci.* **2000**, *5*, 38−43.

(5) Sear, R. P. Interactions in protein solutions. *Curr. Opin. Colloid Interface Sci.* **2006**, *11*, 35−39.

(6) Muschol, M.; Rosenberger, F. Liquid−liquid phase separation in supersaturated lysozyme solutions and associated precipitate formation/crystallization. *J. Chem. Phys.* **1997**, *107*, 1953−1962.

(7) Annunziata, O.; Ogun, O.; Benedek, G. B. Observation of liquid−liquid phase separation for eye lens γS-crystallin. *Proc. Natl. Acad. Sci. U.S.A.* **2003**, *100*, 970−974.

(8) Asherie, N. Protein crystallization and phase diagrams. *Methods* **2004**, *34*, 266−272.

(9) Galkin, O.; Chen, K.; Nagel, R. L.; Hirsch, R. E.; Vekilov, P. G. Liquid−liquid separation in solutions of normal and sickle cell hemoglobin. *Proc. Natl. Acad. Sci. U.S.A.* **2002**, *99*, 8479−8483.

(10) Pande, A.; Pande, J.; Asherie, N.; Lomakin, A.; Ogun, O.; King, J.; Benedek, G. B. Crystal cataracts: Human genetic cataract caused by protein crystallization. *Proc. Natl. Acad. Sci. U.S.A.* **2001**, *98*, 6116−6120.

(11) Wang, Y.; Lomakin, A.; McManus, J. J.; Ogun, O.; Benedek, G. B. Phase behavior of mixtures of human lens proteins Gamma D and Beta B1. *Proc. Natl. Acad. Sci. U.S.A.* **2010**, *107*, 13282−13287.

(12) Lutsko, J. F.; Nicolis, G. Theoretical Evidence for a Dense Fluid Precursor to Crystallization. *Phys. Rev. Lett.* **2006**, *96*, No. 046102.

(13) ten Wolde, P. R.; Frenkel, D. Enhancement of Protein Crystal Nucleation by Critical Density Fluctuations. *Science* **1997**, *277*, 1975−1978.

(14) Piazza, R. Protein interactions and association: an open challenge for colloid science. *Curr. Opin. Colloid Interface Sci.* **2004**, *8*, 515−522.

(15) Curtis, R. A.; Blanch, H. W.; Prausnitz, J. M. Calculation of Phase Diagrams for Aqueous Protein Solutions. *J. Phys. Chem. B* **2001**, *105*, 2445−2452.

(16) Curtis, R. A.; Prausnitz, J. M.; Blanch, H. W. Protein−protein and protein−salt interactions in aqueous protein solutions containing concentrated electrolytes. *Biotechnol. Bioeng.* **1998**, *57*, 11−21.

(17) Collins, K. D. Ions from the Hofmeister series and osmolytes: effects on proteins in solution and in the crystallization process. *Methods* **2004**, *34*, 300−311.

(18) Rosenbaum, D.; Zamora, P.; Zukoski, C. Phase behavior of small attractive colloidal particles. *Phys. Rev. Lett.* **1996**, *76*, 150−153.

(19) Muschol, M.; Rosenberger, F. Interactions in undersaturated and supersaturated lysozyme solutions: Static and dynamic light scattering results. *J. Chem. Phys.* **1995**, *103*, 10424.

(20) Tardieu, A.; Le Verge, A.; Malfois, M.; Bonneté, F.; Finet, S.; Riès-Kautt, M.; Belloni, L. Proteins in solution: from X-ray scattering intensities to interaction potentials. *J. Cryst. Growth* **1999**, *196*, 193−203.

(21) Velev, O. D.; Kaler, E. W.; Lenhoff, A. M. Protein interactions in solution characterized by light and neutron scattering: comparison of lysozyme and chymotrypsinogen. *Biophys. J.* **1998**, *75*, 2682−2697.

(22) Stradner, A.; Sedgwick, H.; Cardinaux, F.; Poon, W. C. K.; Egelhaaf, S. U.; Schurtenberger, P. Equilibrium cluster formation in concentrated protein solutions and colloids. *Nature* **2004**, *432*, 492−495.

(23) Thomson, J. A.; Schurtenberger, P.; Thurston, G. M.; Benedek, G. B. Binary liquid phase separation and critical phenomena in a protein/water solution. *Proc. Natl. Acad. Sci. U.S.A.* **1987**, *84*, 7079−7083.

(24) Liu, Y.; Fratini, E.; Baglioni, P.; Chen, W.-R.; Chen, S.-H. Effective Long-Range Attraction between Protein Molecules in Solutions Studied by Small Angle Neutron Scattering. *Phys. Rev. Lett.* **2005**, *95*, No. 118102.

(25) Hagen, M. H. J.; Frenkel, D. Determination of phase diagrams for the hard-core attractive Yukawa system. *J. Chem. Phys.* **1994**, *101*, 4093−4097.

(26) Asherie, N.; Lomakin, A.; Benedek, G. B. Phase diagram of colloidal solutions. *Phys. Rev. Lett.* **1996**, *77*, 4832−4835.

(27) Noro, M. G.; Frenkel, D. Extended corresponding-states behavior for particles with variable range attractions. *J. Chem. Phys.* **2000**, *113*, 2941−2944.

(28) Platten, F.; Hansen, J.; Wagner, D.; Egelhaaf, S. U. Second Virial Coefficient As Determined from Protein Phase Behavior. *J. Phys. Chem. Lett.* **2016**, *7*, 4008−4014.

(29) Gripon, C.; Legrand, L.; Rosenman, I.; Vidal, O.; Robert, M. C.; Boué, F. Lysozyme Solubility in H_2O and D_2O Solutions: A Simple Relationship. *J. Cryst. Growth* **1997**, *177*, 238−247.

(30) Bucciarelli, S.; Mahmoudi, N.; Casal-Dujat, L.; Jéhannin, M.; Jud, C.; Stradner, A. Extended Law of Corresponding States Applied

DOI: 10.1021/acs.jpcb.6b12814
J. Phys. Chem. B 2017, 121, 1731−1739

to Solvent Isotope Effect on a Globular Protein. *J. Phys. Chem. Lett.* **2016**, *7*, 1610−1615.
(31) Efimova, Y. M.; Haemers, S.; Wierczinski, B.; Norde, W.; Well, A. A. V. Stability of Globular Proteins in H2O and D2O. *Biopolymers* **2007**, *85*, 264−273.
(32) Parker, M. J.; Dempsey, C. E.; Lorch, M.; Clarke, A. R. Acquisition of Native β-Strand Topology During the Rapid Collapse Phase of Protein Folding. *Biochemistry* **1997**, *36*, 13396−13405.
(33) Fu, L.; Villette, S.; Petoud, S.; Fernandez-Alonso, F.; Saboungi, M.-L. H/D Isotope Effects in Protein Thermal Denaturation: The Case of Bovine Serum Albumin. *J. Phys. Chem. B* **2011**, *115*, 1881−1888.
(34) Antonino, L. C.; Kautz, R. A.; Takayuki, N.; Fox, R. O.; Fink, A. L. Cold denaturation and ^2H_2O stabilization of a staphylococcal nuclease mutant. *Proc. Natl. Acad. Sci. U.S.A.* **1991**, *88*, 7715−7718.
(35) Huyghues-Despointes, B. M. P.; Scholtz, J. M.; Pace, C. N. Protein conformational stabilities can be determined from hydrogen exchange rates. *Nat. Struct. Biol.* **1999**, *6*, 910−912.
(36) Cho, Y.; Sagle, L. B.; Limura, S.; Zhang, Y.; Kherb, J.; Chilkoti, A.; Scholtz, J. M.; Cremer, P. S. Hydrogen Bonding of β-Turn Structure Is Stabilized in D2O. *J. Am. Chem. Soc.* **2009**, *131*, 15188−15193.
(37) Jasnin, M.; Moulin, M.; Haertlein, M.; Zaccai, G.; Tehei, M. In Vivo Measurement of Internal and Global Macromolecular Motions in *Escherichia coli*. *Biophys. J.* **2008**, *95*, 857−864.
(38) Gripon, C.; Legrand, L.; Rosenman, I.; Vidal, O.; Robert, M. C.; Boué, F. Lysozyme-lysozyme interactions in under- and supersaturated solutions: a simple relation between the second virial coefficients in H_2O and D_2O. *J. Cryst. Growth* **1997**, *178*, 575−584.
(39) Broutin, I.; Riès-Kautt, M.; Ducruix, A. Lysozyme solubility in H_2O and D_2O solutions as a function of sodium chloride concentration. *J. Appl. Crystallogr.* **1995**, *28*, 614−617.
(40) Platten, F.; Valadez-Pérez, N. E.; Castañeda Priego, R.; Egelhaaf, S. U. Extended law of corresponding states for protein solutions. *J. Chem. Phys.* **2015**, *142*, No. 174905.
(41) Zhang, F.; Skoda, M. W. A.; Jacobs, R. M. J.; Zorn, S.; Martin, R. A.; Martin, C. M.; Clark, G. F.; Weggler, S.; Hildebrandt, A.; Kohlbacher, O.; et al. Reentrant Condensation of Proteins in Solution Induced by Multivalent Counterions. *Phys. Rev. Lett.* **2008**, *101*, No. 148101.
(42) Zhang, F.; Weggler, S.; Ziller, M. J.; Ianeselli, L.; Heck, B. S.; Hildebrandt, A.; Kohlbacher, O.; Skoda, M. W. A.; Jacobs, R. M. J.; Schreiber, F. Universality of protein reentrant condensation in solution induced by multivalent metal ions. *Proteins* **2010**, *78*, 3450−3457.
(43) Roosen-Runge, F.; Heck, B. S.; Zhang, F.; Kohlbacher, O.; Schreiber, F. Interplay of pH and Binding of Multivalent Metal Ions: Charge Inversion and Reentrant Condensation in Protein Solutions. *J. Phys. Chem. B* **2013**, *117*, 5777−5787.
(44) Zhang, F.; Roosen-Runge, F.; Sauter, A.; Wolf, M.; Jacobs, R. M. J.; Schreiber, F. Reentrant Condensation, Liquid-Liquid Phase Separation and Crystallization in Protein Solutions Induced by Multivalent Metal Ions. *Pure Appl. Chem.* **2014**, *86*, 191−202.
(45) Roosen-Runge, F.; Zhang, F.; Schreiber, F.; Roth, R. Ion-activated Attractive Patches as a Mechanism for Controlled Protein Interactions. *Sci. Rep.* **2014**, *4*, No. 7016.
(46) Zhang, F.; Roth, R.; Wolf, M.; Roosen-Runge, F.; Skoda, M. W. A.; Jacobs, R. M. J.; Sztucki, M.; Schreiber, F. Charge-controlled metastable liquid-liquid phase separation in protein solutions as a universal pathway towards crystallization. *Soft Matter* **2012**, *8*, 1313−1316.
(47) Zhang, F.; Zocher, G.; Sauter, A.; Stehle, T.; Schreiber, F. Novel approach to controlled protein crystallization through ligandation of yttrium cations. *J. Appl. Crystallogr.* **2011**, *44*, 755−762.
(48) Zhang, F.; Roosen-Runge, F.; Skoda, M. W. A.; Jacobs, R. M. J.; Wolf, M.; Callow, P.; Frielinghaus, H.; Pipich, V.; Prevost, S.; Schreiber, F. Hydration and interactions in protein solutions containing concentrated electrolytes studied by small-angle scattering. *Phys. Chem. Chem. Phys.* **2012**, *14*, 2483−2493.
(49) Soraruf, D.; Roosen-Runge, F.; Grimaldo, M.; Zanini, F.; Schweins, R.; Seydel, T.; Zhang, F.; Roth, R.; Oettel, M.; Schreiber, F. Protein cluster formation in aqueous solution in the presence of multivalent metal ions - a light scattering study. *Soft Matter* **2014**, *10*, 894−902.
(50) Matsarskaia, O.; Braun, M. K.; Roosen-Runge, F.; Wolf, M.; Zhang, F.; Roth, R.; Schreiber, F. Cation-induced Hydration Effects Cause Lower Critical Solution Temperature Behavior in Protein Solutions. *J. Phys. Chem. B* **2016**, *120*, 7731−7736.
(51) Kubíčková, A.; Křížek, T.; Coufal, P.; Vazdar, M.; Wernersson, E.; Heyda, J.; Jungwirth, P. Overcharging in Biological Systems: reversal of Electrophoretic Mobility of Aqueous Polyaspartate by Multivalent Cations. *Phys. Rev. Lett.* **2012**, *108*, No. 186101.
(52) Fujihara, S.; Akiyama, R. Attractive interaction between macroanions mediated by multivalent cations in biological fluids. *J. Mol. Liq.* **2014**, *200*, 89−94.
(53) Akiyama, R.; Yamashita, T.; Fujihara, S. Hidden peak of radial distribution function and effective attraction between like-charged proteins caused by translational motion of solvent molecules. *J. Mol. Liq.* **2014**, *200*, 72−76.
(54) Akiyama, R.; Sakata, R. An Integral Equation Study of Reentrant Behavior in Attractive Interactions between Like−Charged Macroions Immersed in an Electrolyte Solution. *J. Phys. Soc. Jpn.* **2011**, *80*, No. 123602.
(55) Jordan, E.; Roosen-Runge, F.; Leibfarth, S.; Zhang, F.; Sztucki, M.; Hildebrandt, A.; Kohlbacher, O.; Schreiber, F. Competing Salt Effects on Phase Behavior of Protein Solutions: Tailoring of Protein Interaction by the Binding of Multivalent Ions and Charge Screening. *J. Phys. Chem. B* **2014**, *118*, 11365−11374.
(56) Narayanan, T. Synchroton Small-Angle X-Ray Scattering. In *Soft Matter Characterization*; Borsali, R., Pecora, R., Eds.; Springer: New York, 2008; Chapter 17.
(57) Ianeselli, L.; Zhang, F.; Skoda, M. W. A.; Jacobs, R. M. J.; Martin, R. A.; Callow, S.; Prévost, S.; Schreiber, F. Protein-protein interactions in ovalbumin solutions studied by small-angle scattering: effect of ionic strength and the chemical nature of cations. *J. Phys. Chem. B* **2010**, *114*, 3776−3783.
(58) Kline, S. R. Reduction and analysis of SANS and USANS data using IGOR Pro. *J. Appl. Crystallogr.* **2006**, *39*, 895−900.
(59) Baxter, R. J. Percus-Yevick Equation for Hard Spheres with Surface Adhesion. *J. Chem. Phys.* **1968**, *49*, 2770−2774.
(60) Menon, S. V. G.; Manohar, C.; Rao, K. S. A new interpretation of the sticky hard sphere model. *J. Chem. Phys.* **1991**, *95*, 9186−9190.
(61) Vliegenthart, G. A.; Lekkerkerker, H. N. W. Predicting the gas−liquid critical point from the second virial coefficient. *J. Chem. Phys.* **2000**, *112*, 5364−5369.
(62) Wolf, M.; Roosen-Runge, F.; Zhang, F.; Roth, R.; Skoda, M. W.; Jacobs, R. M.; Sztucki, M.; Schreiber, F. Effective interactions in protein−salt solutions approaching liquid−liquid phase separation. *J. Mol. Liq.* **2014**, *200*, 20−27.
(63) Sauter, A.; Roosen-Runge, F.; Zhang, F.; Lotze, G.; Jacobs, R. M. J.; Schreiber, F. Real-Time Observation of Nonclassical Protein Crystallization Kinetics. *J. Am. Chem. Soc.* **2015**, *137*, 1485−1491.
(64) Sauter, A.; Oelker, M.; Zocher, G.; Zhang, F.; Stehle, T.; Schreiber, F. Nonclassical Pathways of Protein Crystallization in the Presence of Multivalent Metal Ions. *Cryst. Growth Des.* **2014**, *14*, 6357−6366.
(65) Soper, A. K.; Benmore, C. J. Quantum Differences between Heavy and Light Water. *Phys. Rev. Lett.* **2008**, *101*, No. 065502.
(66) Scheiner, S.; Čuma, M. Relative Stability and of Hydrogen and Deuterium Bonds. *J. Am. Chem. Soc.* **1996**, *118*, 1511−1521.
(67) Steiner, T. The Hydrogen Bond in the Solid State. *Angew. Chem., Int. Ed.* **2002**, *41*, 48−76.
(68) Némethy, G.; Scheraga, H. A. Structure of Water and Hydrophobic Bonding in Proteins. IV. The Thermodynamic Properties of Liquid Deuterium Oxide. *J. Chem. Phys.* **1964**, *41*, 680−689.
(69) Kujawa, P.; Winnik, F. M. Volumetric Studies of Aqueous Polymer Solutions Using Pressure Perturbation Calorimetry: A New Look at the Temperature-Induced Phase Transition of Poly(N-

DOI: 10.1021/acs.jpcb.6b12814
J. Phys. Chem. B 2017, 121, 1731−1739

isopropylacrylamide) in Water and D_2O. *Macromolecules* **2001**, *34*, 4130−4135.
(70) Zhang, Y.; Furyk, S.; Bergbreiter, D. E.; Cremer, P. S. Specific Ion Effects on the Water Solubility of Macromolecules: PNIPAM and the Hofmeister Series. *J. Am. Chem. Soc.* **2005**, *127*, 14505−14510.
(71) Moelbert, S.; De Los Rios, P. Hydrophobic Interaction Model for Upper and Lower Critical Solution Temperatures. *Macromolecules* **2003**, *36*, 5845−5853.

DOI: 10.1021/acs.jpcb.6b12814
J. Phys. Chem. B 2017, 121, 1731−1739